Revised submission to Earth and Planetary Science Letters

Measuring multiple cosmogenic nuclides in glacial cobbles sheds light on Greenland Ice Sheet processes

Lee B. Corbett*[a], Paul R. Bierman[a], Thomas A. Neumann[b], Joseph A. Graly[c], Jeremy D. Shakun[d]
Brent M. Goehring[e], Alan J. Hidy[f], and Marc W. Caffee[g,h]

*Corresponding Author: Ashley.Corbett@uvm.edu, (802) 380-2344
[a]Department of Geology, University of Vermont, Burlington, VT, USA
[b]Cryospheric Sciences Laboratory, NASA Goddard Space Flight Center, Greenbelt, MD, USA
[c]Department of Geography and Environmental Sciences, Northumbria University, Newcastle-upon-Tyne, UK
[d]Department of Earth and Environmental Sciences, Boston College, Boston, MA, USA
[e]Department of Earth and Environmental Sciences, Tulane University, New Orleans, LA, USA
[f]Center for Accelerator Mass Spectrometry, Lawrence Livermore National Laboratory, Livermore, CA, USA
[g]Department of Physics and Astronomy, Purdue University, West Lafayette, IN, USA
[h]Department of Earth, Atmospheric, and Planetary Sciences, Purdue University, West Lafayette, IN, USA

Abstract

The behavior of the Greenland Ice Sheet during the Pleistocene remains uncertain due to the paucity of evidence predating the Last Glacial Maximum. Here, we employ a novel approach, cosmogenic nuclide analysis of individual subglacial-derived cobbles, which allows us to make inferences about ice sheet processes and subglacial erosion. From three locations in western Greenland, we collected 86 cobbles from the current ice sheet margin and nine cobbles exposed on the modern proglacial land surface. We measured the concentration of in situ ^{10}Be in all cobbles (n = 95) and ^{26}Al and ^{14}C in a subset (n= 14). Cobbles deposited during Holocene retreat have ^{10}Be exposure ages generally consistent with the timing of ice retreat determined by other methods. Conversely, most of the 86 subglacial cobbles contain very low concentrations of ^{10}Be (median 1.0 x 10^3 atoms g^{-1}), although several have ~10^4 and one has ~10^5 atoms g^{-1}. The low concentrations of ^{10}Be in most subglacial cobbles imply that their source areas under the Greenland Ice Sheet are deeply eroded, preserving minimal evidence of surface or near-surface exposure. The presence of measurable ^{14}C in ten of the cobbles requires that they experienced cosmogenic nuclide production within the past ~30 ka; however, ^{14}C/^{10}Be ratios of ~6 suggest that nuclide production occurred during shielding by overlying material. Only two of the 86 subglacial cobbles definitively have cosmogenic nuclide concentrations consistent with prior surface exposure. Overall, isotopic analysis of subglacial cobbles indicates that western Greenland's subglacial landscape is characterized by deep erosion and minimal subaerial exposure.

Keywords (n = 6): Cosmogenic nuclides; Greenland; Geochemistry; Isotopes; Pliocene; Pleistocene

1. Introduction

The Greenland Ice Sheet is an erosive agent that has shaped the underlying landscape for millions of years (Bierman et al., 2016). However, the depth of scouring, spatial distribution of erosive versus non-erosive areas, and mechanisms of sediment entrainment and transport remain uncertain due to the inaccessibility of the subglacial landscape. Ice retreat during interglacial periods can expose a limited view of surfaces that are usually covered by ice, and studies of sediments deposited in the marine realm (Bierman et al., 2016; Christ et al., 2019; Flesche-Kleiven et al., 2002; Helland and Holmes, 1997; Larsen et al., 1994) provide an offshore view of glacial processes. Analysis of bedrock at the bottom of ice cores (Schaefer et al., 2016) provides a direct sampling of the subglacial landscape, albeit at a single point in space. But overall, studies of the subglacial landscape remain limited and often rely on fragmentary and indirect evidence.

Here, we seek to assess long-term ice sheet behavior and erosivity using a novel approach: analysis of multiple cosmogenic nuclides in individual detrital cobbles sourced from beneath the Greenland Ice Sheet and transported to the ice margin by ice and/or subglacial water. We use 86 subglacial cobbles collected from the modern-day ice sheet margin and proximal outwash streams as well as nine cobbles from the proglacial landscape (Fig. 1 and Supplementary Data Fig. S1), the cosmogenic nuclide concentrations of which record ice sheet processes over both time and space. The cobbles come from three regions in western Greenland with distinct glaciological and erosive conditions.

Quantifying cosmogenic nuclide concentrations in detrital cobbles instead of at a single location (e.g., bedrock from the GISP2 ice core, Schaefer et al. (2016)) provides wide spatial

coverage, allowing us to infer ice sheet processes across extensive subglacial sediment source areas. Although the source location and flow path of any individual cobble is unknowable and the exposure and erosion history cannot be modeled uniquely, investigating a large number of cobbles yields patterns and trends in cosmogenic nuclide concentrations. We assess these patterns in subglacial cobble cosmogenic nuclide concentrations to make inferences about western Greenland Ice Sheet processes.

2. Background

2.1. Using Multiple Cosmogenic Nuclides to Infer Cobble Exposure/Erosion History

In situ produced cosmogenic nuclides, such as ^{10}Be, ^{26}Al, and ^{14}C, have been employed for several decades to reconstruct glacial histories of bedrock surfaces and moraine boulders (Balco, 2011). These nuclides, produced predominately by secondary neutron spallation reactions (Lal and Peters, 1967) but also by muon interactions (Heisinger et al., 2002a; Heisinger et al., 2002b) build up in rock at known rates over time. Because production by neutron spallation decreases exponentially with depth, subglacial erosion of several meters of rock strips most pre-existing spallation-produced nuclides (Balco, 2011). Production by muon interactions (Heisinger et al., 2002a; Heisinger et al., 2002b) occurs at lower rates but to a greater depth, such that muon-produced nuclides are present in rocks at low but measurable concentrations even after glacial erosion has stripped tens of meters of surface material (Bierman et al., 2016; Briner et al., 2016; Davis et al., 1999).

When multiple cosmogenic nuclides with different half-lives (e.g. ^{10}Be, 1.4 Ma; ^{26}Al, 0.7 Ma; and ^{14}C, 5.7 ka) are analyzed in the same sample, ratios of their concentrations provide

67 information about both exposure and burial (Briner et al., 2014). Nuclide production dominates
68 the former, whereas loss through radioactive decay dominates the latter. Pairing two longer-
69 lived nuclides, such as $^{26}Al/^{10}Be$, provides information about exposure and burial integrated
70 over the past 10^5 to 10^6 years (Balco et al., 2014), but is relatively insensitive to short durations
71 of burial (less than several hundred kyr). Shorter-lived nuclides, such as ^{14}C, are more sensitive
72 to recent exposure, burial, and erosion (Briner et al., 2014; Miller et al., 2006). Because the ^{14}C
73 half-life is two orders of magnitude less than those of ^{10}Be and ^{26}Al, appreciable ^{14}C mandates
74 spallation and/or muon production within ~30 ka.
75 Such multi-isotope approaches depend on knowing the ratio of the isotopes during
76 surface production. For $^{26}Al/^{10}Be$, the ratio of surface production is generally assumed to be
77 ~6.75 (Balco et al., 2008), although recent modeling (Argento et al., 2013) and empirical data
78 (Corbett et al., 2017) suggest that the value may be higher in certain locations. For $^{14}C/^{10}Be$, the
79 ratio of surface production, albeit less well-constrained, is ~3-4 (Argento et al., 2013; Briner et
80 al., 2014; Schimmelpfennig et al., 2012). Ratios lower than production are indicative of burial
81 following initial exposure, or of prolonged surface exposure because the ratio decreases over
82 time due to preferential decay of the shorter-lived nuclide.
83 Because the production rates and ratios are dependent on depth, the ratios change as a
84 result of the relative proportion of the spallogenic and muogenic production (as reviewed in
85 Marrero et al. (2016)). Accounting for their respective instantaneous production pathways, the
86 $^{26}Al/^{10}Be$ production ratio increases only slightly with depth, whereas the $^{14}C/^{10}Be$ and $^{14}C/^{26}Al$
87 production ratios increase more appreciably with depth (Fig. 2). This occurs because the
88 muogenic fraction of the total is greater for ^{14}C than for ^{10}Be and ^{26}Al (Lupker et al., 2015).

Therefore, although $^{14}C/^{10}Be$ and $^{14}C/^{26}Al$ are generally used to assess burial following initial exposure (Briner et al., 2014; Miller et al., 2006), nuclide ratios can also be used to assess shielding depth during exposure (Rand and Goehring, 2019).

2.2. Greenland Ice Sheet Processes and Implications for Subglacial Cobble Nuclide Concentrations

2.2.1. Ice Sheet History and Possible Subglacial Cobble Exposure Periods

Although continental glaciation occurred as early as the middle to late Miocene in East Greenland (Helland and Holmes, 1997; Larsen et al., 1994), expansive ice likely first occupied Greenland ~2.5 Ma, coincident with overall northern hemisphere cooling (Bierman et al., 2016; Flesche-Kleiven et al., 2002). Since the inception of a large Greenland Ice Sheet at the beginning of the Pleistocene, Greenland's landscape has been dominated by burial and progressive erosion rather than exposure (Bierman et al., 2016).

In addition to being exposed to cosmic rays before the onset of glaciation (with varying degrees of partial shielding based on their depth of burial), the cobbles or their source outcrops could have been re-exposed when ice extent was reduced during warm periods of the Pleistocene (Schaefer et al., 2016). Interglacial sediments indicative of a warm Arctic exist in several locations around Greenland and are thought to be early Pleistocene in age (Funder et al., 2001). During MIS11 at ~400 ka, pollen evidence (De Vernal and Hillaire-Marcel, 2008) and sediment provenance studies (Reyes et al., 2014) show that much of the southern Greenland Ice Sheet disappeared. The Eemian Period ~130 ka was characterized by appreciably reduced ice extent as suggested by marine sediment provenance (Colville et al., 2011) and modeling

(Helsen et al., 2013). Finally, the Greenland Ice Sheet was smaller than present for several thousand years during the warm middle Holocene as evidenced by lake sediment core records (Briner et al., 2010; Larsen et al., 2015).

Although nuclide production in the cobbles we analyzed could have occurred via neutron spallation during exposure in conjunction with these warm periods, muon production also decidedly occurred at depths of meters to tens of meters in the absence of surface exposure. Because muon production extends many meters through overlying material (Heisinger et al., 2002a; Heisinger et al., 2002b), nuclides would have been produced deep within cobble source outcrops before the onset of glaciation and in cobbles or source outcrops beneath overlying till, ice, or snow.

2.2.2. Glaciological Processes, Subglacial Erosion, and Cobble Plucking

In addition to recording ice sheet history, the cosmogenic nuclide concentrations of the cobbles we sampled are the result of ice sheet processes including subglacial erosion, plucking, freeze-on, and transport. The Greenland Ice Sheet likely began eroding parts of the underlying landscape as soon as glaciation began, and erosion continued throughout the Pliocene and Pleistocene, progressively eroding through the preglacial regolith and into bedrock at least in certain areas (Bierman et al., 2016). Cobbles were likely sourced from areas that at some point had basal temperatures at or near the pressure-melting point, in order for regelation to incorporate the cobbles into the ice matrix (Alley et al., 1997). However, basal conditions of the Greenland Ice Sheet are not well documented over space and time, and closely juxtapose warm-based (erosive) and cold-based (non-erosive) ice (Petrunin et al., 2013). This spatial and

temporal heterogeneity means that cobble source areas likely changed over time along with bed conditions.

The residence time of cobbles and sediment in the basal ice is largely determined by the relationships between the basal thermal state, the ice thickness, and the vertical and horizontal flow velocity. Cobbles are either incorporated into or shed from the ice depending on the thermal state at the ice-bed interface (Cuffey and Paterson, 2010). The along-flow advection rates of material within the ice varies from near zero at the ice sheet center to hundreds of meters per year near the margin (Cuffey and Paterson, 2010). These rates of advection and the incorporation or deposition of cobbles evolve through time owing to changes in ice sheet conditions, which are constantly re-adjusting in response to changing climate.

3. Study Sites

Our study focuses on three locations in western Greenland: Kangerlussuaq, Ilulissat, and Upernavik (Fig. 1). We chose these three sites because their contrasting landscapes are indicative of different glacial processes and erosive regimes. The chronology of ice retreat and the likely timing of surficial cobble exposure is constrained by previous work at each of the three sites.

In Kangerlussuaq (67°N, -50°E), the landscape morphology and existing cosmogenic nuclide data are suggestive of deep glacial erosion. The region is characterized by a glacially-sculpted landscape of NE-SW elongated hills and lakes, carved parallel to the direction of ice flow. Rounded, striated bedrock is common. Till fills the valleys, whereas hilltops are typically bare rock. Numerous Holocene moraines are preserved; ^{10}Be analyses of moraine boulders

(Levy et al., 2012) cluster and are consistent with the local organic radiocarbon chronology, suggesting no or minimal inheritance of nuclides from previous exposure periods. Similarly, $^{26}Al/^{10}Be$ analyses of high-elevation bedrock surfaces in the area generally indicate deep erosion followed by a single period of exposure during the Holocene (Beel et al., 2016). Meteoric ^{10}Be concentrations in the fine-grained glacial sediment at Kangerlussuaq (n=17) are significantly lower than in other regions of Greenland, suggestive of effective subglacial erosion (Graly et al., 2018). The deposition of the three surficial cobbles we measured likely occurred ~6.8 ka based on the moraine chronology of Levy et al. (2012).

In Ilulissat (69°N, -50°E), the land surface and previously published cosmogenic nuclide data both suggest extensive glacial erosion, similar to in Kangerlussuaq. The landscape is glacially sculpted, heavily striated, and cut by numerous fjords. Most of the ice in the region drains through a large ice stream, Jakobshavn Isbræ. Holocene moraines are present and dozens of cosmogenic nuclide analyses (reviewed in Young et al. (2013)) suggest that ^{10}Be inheritance from previous exposure is minimal. The deposition of the three surficial cobbles we measured likely occurred ~7.8 ka based on the ages of a bedrock sample (GL080; 7.9 ± 0.2 ka) and a boulder sample (GL081; 7.6 ± 0.1 ka) collected from the same location as the cobbles (Corbett et al., 2011).

In Upernavik (~72°N, -54°E), unlike Kangerlussuaq and Ilulissat, the landscape morphology and existing cosmogenic nuclide data indicate that glacial erosion was heterogeneous and limited. The region has large relief, characterized by table-top highlands cut by deep fjords. Although some low-elevation bedrock surfaces exhibit glacial rounding, the highlands show evidence of prolonged subaerial weathering including exfoliation, tors, and

weathering pits. Analysis of ^{10}Be and ^{26}Al in Upernavik (Corbett et al., 2013) and south of Upernavik (Beel et al., 2016) indicates that the ice was cold-based and non-erosive at times in the past. At high elevations, multi-isotope analysis shows that surfaces preserve total histories of ~10^5-10^6 years, and even some low-elevation surfaces contain nuclides inherited from periods of exposure prior to the Holocene (Beel et al., 2016; Corbett et al., 2013). Meteoric ^{10}Be concentrations of fine-grained sediment entrained in the ice margin are higher here than in Kangerlussuaq or Ilulissat (Graly et al., 2018). The deposition of the three surficial cobbles we measured (collected from an upland surface proximal to the ice margin) may have occurred ~12.1 ka based on the mean of ages from a bedrock sample (GU001; 13.6 $\pm$ 0.3 ka) and a boulder sample (GU002; 10.6 $\pm$ 0.3 ka) collected from the same location, or ~11 ka based on our best deglaciation estimate for the region (Corbett et al., 2013), although all of these estimates may be inflated by the presence of inherited ^{10}Be.

4. Methods

4.1. Study Design and Sample Collection

We measured in situ cosmogenic nuclides (^{10}Be in all; ^{26}Al and ^{14}C in a subset) in 86 subglacial cobble-sized rocks from Kangerlussuaq (n=33), Ilulissat (n=20), and Upernavik (n=33) (Fig. 1, Supplementary Data Table S1). Most of these cobbles ("icebound cobbles", n = 62) were sourced from sediment-laden basal ice exposed at the ice sheet margin or supraglacial debris bands not near nunataks (Figs. S1A, S1B, S1C), while a smaller portion ("outwash cobbles", n = 24) were sourced from ice-proximal channels just outside of large outwash tunnels (Fig. S1D). We recorded information about cobble size, lithology, and angularity, and measured the

location of collection with a hand-held GPS (Table S1). Cobble lithologies vary, although most are quartz-rich crystalline rocks including granite and gneiss; a much smaller portion are quartzite, breccia, and schist.

We also analyzed ^{10}Be in an additional three surficial cobbles from each site (n = 9 total, detailed in Table S1, Figs. S1E and S1F) from the modern proglacial landscape to assess whether inherited ^{10}Be is detectable in samples that have been exposed since deglaciation. At two sites, Ilulissat and Upernavik, we collected the surficial cobbles directly adjacent to a bedrock-boulder sample pair. We purposefully selected cobbles of similar sizes to those collected at the ice margin so that the two populations are comparable. At all three sites, the surficial cobbles came from local topographic highpoints with little/no present-day sediment or vegetation cover. At each site, the cobbles were collected within close proximity of each other, usually a few meters.

4.2. Sample Preparation and Analysis

Additional methodological detail can be found in the Supplementary Data and in Tables S1-S5. For ^{10}Be and ^{26}Al, Samples were prepared at University of Vermont using procedures described in Corbett et al. (2016). ^{10}Be/^{9}Be ratios were measured by accelerator mass spectrometry (AMS) at Lawrence Livermore National Laboratory and corrected for backgrounds using a ^{10}Be/^{9}Be blank ratio of $(4.2 \pm 1.6)\cdot10^{-16}$ (n = 24, Table S3). We chose a threshold ^{10}Be concentration of $3\cdot10^{3}$ atoms g^{-1} (exceeded by 14 of the 86 subglacial cobbles), above which we also analyzed ^{26}Al and ^{14}C. This analytical threshold was chosen to select for samples with sufficient ^{26}Al to be measurable above detection limits and to yield meaningful ^{26}Al/^{10}Be ratios. ^{26}Al/^{27}Al ratios were measured by AMS at Purdue Rare Isotope Measurement (PRIME)

Laboratory and corrected for backgrounds using a $^{26}Al/^{27}Al$ blank ratio of $(7.6 \pm 7.0)\cdot10^{-16}$ (n = 14, Table S3). For ^{14}C, sample preparation and measurement by AMS were conducted at University of Cologne (Fulop et al. (2015), Table S4).

For the nine surficial cobbles, we calculated exposure ages (Table S5) with the CRONUS Earth online exposure age calculator (Balco et al., 2008). We used the northeastern North American production rate calibration dataset and Lal/Stone scaling (see Supplementary Data for details).

4.3. Theoretical Models

To explore the concentrations of ^{10}Be and ^{26}Al under a long-lived, erosive ice sheet, we modeled the evolution of their concentrations in a bedrock profile for various erosion, exposure, and ice thickness scenarios. We assumed sea-level high-latitude production rates, including production by muons, calculated using the MATLAB implementation in Balco et al. (2008) of the method of Heisinger et al. (2002b) and a $^{26}Al/^{10}Be$ surface production ratio of 7.3 (Corbett et al., 2017). The simulations were initialized with a bedrock profile in steady state (i.e., nuclide production equal to nuclide loss from decay and erosion), based on various constant preglacial erosion rates (5, 20, and 50 m Myr^{-1}) assuming no ice cover prior to the Pleistocene. We then considered two exposure scenarios following the onset of glaciation at 2.5 Ma: (1) continuous ice cover and (2) 8 kyr of interglacial exposure every 100 kyr (i.e., scenario 2 in Schaefer et al. (2016), their Fig. 3). The sensitivity of results to muon production through ice was examined for a range of ice thicknesses (50 m, 200 m, 1000 m, and infinite) during intervals of cover. We modeled erosion by removing surface material and shifting the profile up in

243 proportion to the subglacial erosion rate (5, 20, and 50 m Myr^{-1}) when ice covered, and
244 assumed zero erosion when ice free. Nuclides experience continuous decay throughout each
245 simulation.
246
247 **5. Results**
248 For the 73 subglacial cobbles with $^{10}Be/^{9}Be$ detectable above background values, ^{10}Be
249 concentrations are $(2.0 \pm 1.0)\cdot10^{2}$ to $(1.12 \pm 0.02)\cdot10^{5}$ atoms g^{-1} (Table S1), ranging over three
250 orders of magnitude. The ^{10}Be concentrations form a right-skewed distribution with a median
251 of $1.0\cdot10^{3}$ atoms g^{-1} and a mean of $4.2\cdot10^{3}$ atoms g^{-1} (Fig. 3). The ^{10}Be concentrations do not
252 form statistically separable populations (Fig. 4) based on type (icebound vs. outwash; t-test, p =
253 0.29), location (Kangerlussuaq, Ilulissat, Upernavik; ANOVA, p = 0.67), shape (angular,
254 subangular, subrounded, rounded; ANOVA, p = 0.46), or lithology (gneiss, granite, other;
255 ANOVA, p = 0.81).
256 The 14 subglacial cobbles with the highest ^{10}Be concentrations (>$3\cdot10^{3}$ atoms g^{-1}, the
257 analytical threshold used to determine which samples we analyzed for ^{26}Al and ^{14}C) also do not
258 cluster with regards to cobble characteristics (Table S1). They have varying lithologies and
259 varying shapes, ranging from subrounded to angular, although none of the 14 were well-
260 rounded. They came from both the ice margin itself as well as outwash deposits, with no
261 systematic bias toward one or the other.
262 ^{26}Al concentrations are $(2.3 \pm 0.3)\cdot10^{4}$ to $(7.7 \pm 0.3)\cdot10^{5}$ atoms g^{-1} and the resulting
263 $^{26}Al/^{10}Be$ ratios are 5.0 ± 1.1 to 8.4 ± 1.2 (n = 13, Tables 1 and S2, Fig. 5). In reference to the
264 empirically-determined Greenland $^{26}Al/^{10}Be$ surface production ratio of 7.3 (Corbett et al.,

2017), none of the cobbles are above the production ratio by >1σ, 7 are indistinguishable, and 6 are below by >1σ. Conversely, in reference to the commonly-assumed $^{26}Al/^{10}Be$ surface production ratio of 6.75, 5 cobbles are above by >1σ, 5 are indistinguishable, and 3 are below by >1σ.

Of the cobbles analyzed for ^{14}C, three were below detection limit; the remaining ten ^{14}C concentrations are $(5.1 \pm 1.4)\cdot10^4$ to $(1.5 \pm 0.2)\cdot10^5$ atoms g^{-1} (n = 13, Tables 1 and S4). All but two samples (GK015 and GU010) have significant ^{14}C in excess of the instantaneous $^{14}C/^{10}Be$ surface production ratio (Fig. 6). When $^{14}C/^{10}Be$ and $^{14}C/^{26}Al$ are plotted as regressions, all but the same two of the samples lie along a trendline forming a significant linear relationship (R^2 = 0.92 for both regressions); the slope of the regression is 5.92 for $^{14}C/^{10}Be$ and 0.76 for $^{14}C/^{26}Al$ (Fig. 7), both well above the surface production ratios. The two samples not on the regression (GK015 and GU010) have higher ^{10}Be and ^{26}Al concentrations but lower ^{14}C concentrations than the remainder of the dataset (Fig. 6).

For the nine surficial cobbles, ^{10}Be concentrations are $(3.9 \pm 0.1)\cdot10^4$ to $(6.9 \pm 0.1)\cdot10^4$ atoms g^{-1} (Table S5). The average ^{10}Be concentrations by site are $(4.4 \pm 0.6)\cdot10^4$ for Kangerlussuaq, $(5.4 \pm 0.5)\cdot10^4$ for Ilulissat, and $(5.6 \pm 1.2)\cdot10^4$ for Upernavik (1SD, n = 3 for each), representing relative standard deviations of 12.5, 8.5, and 20.9%, respectively. When considered as exposure ages assuming constant exposure and no erosion, these translate to 6.8 ± 0.8 ka (Kangerlussuaq), 8.1 ± 0.7 ka (Ilulissat), and 7.8 ± 1.6 ka (Upernavik; n = 3, average, 1SD for each, Table S5).

6. Discussion

6.1. Subglacial Cobbles Generally Record Deep Subglacial Erosion

Most of the subglacial cobbles we measured have cosmogenic nuclide concentrations indicating deep erosion under ice without subsequent surface exposure. Long-exposed, high-latitude landscapes, such as the Tertiary preglacial Greenland land surface, would have had ^{10}Be concentrations of ~10^5-10^6 atoms g^{-1}, depending on subaerial erosion rates (see Bierman et al. (2016), their Figs. 2a and 4). The cobbles we measured had much lower ^{10}Be concentrations (13 below detection limit and an additional 37 with <10^3 atoms g^{-1}, Fig. 3), suggesting they were sourced from deeply-eroded outcrops with little exposure to cosmic radiation. Some of the cobbles with low ^{10}Be concentrations may have never experienced exposure at the surface; their nuclide inventories could be due to muogenic production at depth (Heisinger et al., 2002a; Heisinger et al., 2002b) during shielding by overlying rock, sediment, and/or ice. The general lack of ^{10}Be in the samples demonstrates that an uneroded or minimally eroded, subglacially-preserved, Tertiary landscape was not the source material for the cobbles we collected.

However, all glacial detrital sediment records, including the cobbles we studied, are biased toward areas of the ice sheet that generate significant volumes of sediment. The cobbles were most likely derived from areas of warm-based ice, or areas that had warm-based ice during at least one time, in order for plucking or freeze-on to have occurred. This over-representation of erosive areas is similar to biases in records developed from marine sediment cores (Bierman et al., 2016; Christ et al., 2019; Flesche-Kleiven et al., 2002; Helland and Holmes, 1997; Larsen et al., 1994) and studies of sediment emanating from glacial drainages (Nelson et al., 2014). The cobbles therefore resulted from processes operating in sediment source areas

beneath the ice sheet, presumably areas of warm-based and erosive ice, rather than the subglacial landscape as a whole.

Our estimates of subglacial erosion suggest that at least tens to more likely hundreds of meters of rock have been removed from the cobble source landscapes since the onset of glaciation. Theoretical models (Figs. 8, S2, S3) demonstrate that subglacial erosion rates of ~20-50 m Myr^{-1} are needed to drive ^{10}Be concentrations in exhumed material down to 10^3 atoms g^{-1} assuming thick, continuous ice cover since 2.5 Ma (the resulting ^{10}Be concentrations are also sensitive to the assumed preglacial erosion rate, which we varied from 5-50 m Myr^{-1}, Figs. 8, S2). These erosion rates are minimum estimates, however, because our measured $^{26}Al/^{10}Be$ ratios (~5-8, close to that of surface production) and the $^{26}Al/^{10}Be$ of bedrock from the bottom of the GISP2 ice core (~4; Schaefer et al. (2016)) indicate that interior Greenland experienced exposure during the Pleistocene, which would increase nuclide concentrations (Figs. 8, S3). The $^{26}Al/^{10}Be$ ratios we measured are also consistent with muon production through thin, continuous ice cover for the past 2.5 Myr, but greater erosion rates (> 50 m Myr^{-1}) in this case would be required to reduce ^{10}Be concentrations to 10^3 atoms g^{-1} (Figs. 8, S2).

Overall, these findings are consistent with deep subglacial erosion and nuclides produced by muons (whether through thin ice or overlying bedrock) during the Pleistocene. These findings agree well with the quantitative estimates of subglacial erosion of Strunk et al. (2017), who used paired $^{26}Al/^{10}Be$ data from Greenland's coastal landscapes and a Monte Carlo approach tuned to the oxygen isotope record to conclude that low-lying landscapes (i.e. probable source areas for the cobbles we collected) have eroded at >50 m Ma^{-1} during the duration of ice cover. Similarly, Goehring et al. (2010) inferred 2-34 m of erosion during the last

glacial cycle based on ^{10}Be in East Greenland ice-contact delta sediments, implying erosion rates of tens to hundreds of m Myr^{-1}.

6.2. The Greenland Ice Sheet: An (Imperfect) Erosion Machine

Within the spectrum of previously-published cosmogenic measurements of glacial materials in Greenland (see previous studies plotted on Fig. 1), our subglacial cobbles (median 1.0 ·10^3 atoms g^{-1}, mean 4.2 ·10^3 atoms g^{-1}) have ^{10}Be concentrations similar to sand emerging from the present-day subglacial drainage system via outwash streams in southern Greenland (mean = 6.5 ± 4.1 ·10^3 atoms g^{-1}, n = 19, 1SD, Nelson et al. (2014)) and inheritance calculated from eastern Greenland glacial delta depth profiles (error-weighted mean = 6.9 ± 1.0 x 10^3 atoms g^{-1}, n = 5, 1SD, Goehring et al. (2010), their Fig. 8). The detrital sediment assessed by both Nelson et al. (2014) and Goehring et al. (2010) is more similar to the mean than the median of the cobble data we present, likely because subglacial erosion and transport homogenizes sediment, combining material from more- and less-eroded areas, an effect that we mimic with a large number of cobbles.

The ^{10}Be concentrations of Greenland's subglacial sediments (this study, Nelson et al. (2014), and Goehring et al. (2010)) are lower today than they were in the past. Analyses of East Greenland marine cores (Bierman et al., 2016) suggest that sediments shed off Greenland had appreciably more ^{10}Be in the late Miocene and Pliocene (~10^5 atoms g^{-1} with decay correction) and somewhat more ^{10}Be throughout the late Pliocene and early Pleistocene (~10^4 atoms g^{-1} with decay correction), not reaching ~10^3 atoms g^{-1} until about the past 1-2 Ma. Glacial diamict recovered in a west Greenland marine core from ~1.8 Ma has ^{10}Be concentrations as low as our

cobbles (mean= 4.6 ± 2.0 $\cdot 10^3$ atoms g^{-1}, n = 5, 1SD, (Christ et al., 2019)). The general decrease in ^{10}Be concentration over time and the low concentrations of ^{10}Be in Pleistocene and modern subglacial materials portrays the Greenland Ice Sheet as an erosive system that has (at least in certain locations) progressively excavated down into deep, seldom-exposed bedrock or sediments that are now being transported to the margin.

Although cosmogenic nuclide analyses of detrital sediments generally indicate deep glacial erosion, cosmogenic nuclide analyses of in-place bedrock around Greenland demonstrate that the ice sheet erodes its bed in some areas and not in others, highlighting that the cobbles are biased toward deeply eroded sediment source areas. The bottom of the GISP2 ice core from central Greenland preserves bedrock with an order of magnitude more ^{10}Be (9.8-24.8 $\cdot 10^3$ atoms g^{-1}, Schaefer et al. (2016)) than the subglacial cobbles considered here. Around Greenland's margins there are isolated regions of non-eroded bedrock and resulting high concentrations of ^{10}Be, particularly at high elevations where the ice was likely cold-based and non-erosive, as demonstrated in both west (Beel et al., 2016; Corbett et al., 2013) and east (Håkansson et al., 2009) Greenland. Less erosive areas of the ice sheet do exist, both around the margins and in the interior, but are not represented in the detrital record since those uneroded, high-cosmogenic-nuclide-concentration landscapes are still in place.

6.3. Nuclide Production During Shielding

The presence of measurable in situ cosmogenic ^{14}C in the cobbles unequivocally demonstrates recent (within several tens of ka) production of cosmogenic nuclides. Because the half-life of ^{14}C is so short (5.7 ka), any ^{14}C from before ~30 ka has largely decayed away;

thus, the ^{14}C we measured indicates nuclide production during the latest Pleistocene or Holocene. Recent nuclide production is further evidenced by the significant linear relationship between ^{14}C with ^{10}Be and ^{26}Al (Fig. 7), as recent surface or near-surface exposure and the resulting co-production of ^{14}C, ^{10}Be, and ^{26}Al is the only mechanism to produce a correlation between the short-lived and the long-lived nuclides.

It is likely that this nuclide production occurred when the cobbles were partially shielded. The slope of the $^{14}C/^{10}Be$ regression formed by most of the cobbles is 5.9 (R^2 = 0.92, n = 8, Fig. 7), appreciably higher than the commonly accepted surface $^{14}C/^{10}Be$ production ratio of ~3-4 (Argento et al., 2013; Briner et al., 2014; Schimmelpfennig et al., 2012). The higher than expected $^{14}C/^{10}Be$ is explained best by muogenic production during shielding (Rand and Goehring, 2019), likely under a minimum shielding mass of at least ~200-250 g cm^{-2} (Fig. 2). Even four cobbles with no measurable ^{10}Be contain ^{14}C (Fig. 7, see also Supplementary Data for detail), supporting the idea that the cobbles were initially sourced from depth and remained shielded. Because muon production is a larger component of the total production in ^{14}C than in ^{10}Be, it allows for the production of ^{14}C in the near-absence of ^{10}Be production under shielding.

Our results do not provide direct information about the composition of the material that shielded the samples during the past ~30 ka, but we infer that ice is the most likely. The observation that most cobbles (all except GK015 and GU010) fall so closely along a line (Fig. 7) indicates that the cosmogenic nuclides they contain were produced at the same time and under similar shielding conditions. One possibility is that nuclide production occurred under partial shielding during the cobbles' journeys along glacial flow lines that took them upward and outward toward the glacial margin. But regardless of whether shielding occurred by rock,

sediment, ice, or a combination thereof, the high $^{14}C/^{10}Be$ ratios generally reflect a cobble life cycle that is dominated by shielding and nuclide production at depth by muons.

6.4. Interglacial Ice Sheet Retreat and Exposure Preceding the Last Glacial Period

Based on multiple nuclide data, only two of the 86 cobbles we analyzed unambiguously experienced surface or near-surface exposure prior to ~30 ka: GK015 (subangular gneiss from Kangerlussuaq) and GU010 (subangular granodiorite from Upernavik), both of which we collected directly from the ice sheet margin. Both cobbles' $^{14}C/^{10}Be$ ratios can be explained with spallogenic rather than exclusively muogenic production (Figs. 6 and 7). The cobbles must have experienced at least some recent exposure, likely at depth as discussed above and causing them to contain measurable ^{14}C, but they were also exposed prior to ~30 ka.

To assess exposure before ~30 ka, we can correct for recent nuclide production at depth by removing the ^{10}Be and ^{26}Al that would have been co-produced with the measured ^{14}C. We made this correction by using the measured ^{14}C concentration and the slopes of the $^{14}C/^{10}Be$ and $^{14}C/^{26}Al$ regressions to infer the concentrations of ^{10}Be and ^{26}Al that were co-produced with ^{14}C, and subtracting in order to estimate ^{10}Be and ^{26}Al before ~30 ka. This correction yields $^{26}Al/^{10}Be$ ratios of 5.76 ± 0.36 for GK015 and 6.80 ± 0.26 for GU010.

After correcting the ^{10}Be and ^{26}Al concentrations for recent production, the pre-~30 ka exposure/burial histories of these two cobbles likely differ in both duration and timing. For sample GK015, the corrected $^{26}Al/^{10}Be$ ratio (5.76 ± 0.36) is below the $^{26}Al/^{10}Be$ production ratio (regardless of whether we assume a surface production ratio of 7.3 or 6.75) beyond 1σ uncertainties, which could be explained by either burial following exposure or prolonged

419 exposure that caused the $^{26}Al/^{10}Be$ ratio to drop due to the shorter half-life of ^{26}Al (Balco et al.,
420 2014). In the case of the former, initial exposure could not have occurred exclusively during
421 MIS5e because the duration of intervening burial would be insufficient to cause a detectable
422 departure from the production ratio, although it could have been re-exposed during MIS5e in a
423 multi-stage exposure scenario. Sample GU010 has a higher corrected $^{26}Al/^{10}Be$ ratio (6.80 $\pm$
424 0.26), likely indicating surface exposure during a more recent warm period (and perhaps during
425 older periods as well). Its ^{10}Be concentration is the highest of the 86 cobbles we measured,
426 requiring at least ~25 ka of surface exposure at sea level (less at higher elevations); accordingly,
427 this inventory of ^{10}Be could not have built up only during the Holocene Climatic Optimum. Its
428 cosmogenic nuclide inventory is a product of multiple periods of exposure, likely including
429 MIS5e and perhaps previous interglacials as well.
430
431 *6.5. Cosmogenic Nuclide Inheritance and Implications for Dating Studies*
432 Measurable, if low, in situ cosmogenic nuclide concentrations in most subglacial cobbles
433 imply that even extensive, long-lived glacial erosion is unable to fully "reset" the cosmogenic
434 clock (Briner et al., 2016; Davis et al., 1999; Rand and Goehring, 2019). Our dataset provides
435 two complementary lines of evidence for the presence of muon-produced nuclides: (1) low but
436 pervasive ^{10}Be concentrations (median 10^3 atoms g^{-1}) and (2) $^{14}C/^{10}Be$ and $^{14}C/^{26}Al$ co-
437 production at ratios definitively higher than those of surface production. Small concentrations
438 of primarily muon-produced nuclides are likely present in many glacial environments even after
439 extensive subglacial erosion, not only in moraine boulders and glacially-sculpted bedrock as is

frequently observed (Balco, 2011), but also in detrital sediment (Goehring et al., 2010; Nelson et al., 2014).

Although inherited ^{10}Be is probably present in most cobbles transported to the ice sheet margin, its impact on inferred exposure ages depends on the relative portion of inherited ^{10}Be versus ^{10}Be produced during the current period of exposure (Fig. 9). The median subglacial cobble ^{10}Be concentration is ~10^3 atoms g^{-1}, equivalent to about 250 years of surface exposure at high latitude; this represents a relatively small effect on the age of a latest Pleistocene moraine, but a very appreciable effect on the age of a Little Ice Age moraine. However, a subset of the subglacial cobbles we analyzed contained higher ^{10}Be concentrations, which would appreciably skew exposure ages for any dating application; for example, GU010 contains ~10^5 atoms g^{-1} of ^{10}Be, the equivalent of ~25 ky of surface exposure at sea level and high latitude.

The nine surficial cobbles we collected and analyzed exhibit scatter in their ^{10}Be concentrations and inferred ages (Fig. 9, Table S5). ^{10}Be concentrations of these cobbles (n = 3 per site) are not consistent within 1σ analytic uncertainties (Fig. 9), despite being collected within close proximity. Such variance could reflect shielding (e.g., by snow, ice, or till since deposition, which may be more important for small cobbles than for large boulders) and/or the presence of inherited produced ^{10}Be.

Cobble exposure ages (Fig. 9, Table S5) agree with independent estimates of deglaciation timing better in certain locations than in others. In Kangerlussuaq, the mean surficial cobble age (6.8 ± 0.8 ka; Fig. 9) is consistent with the age of deglaciation inferred from the moraine chronology of Levy et al. (2012). In Ilulissat, the mean surficial cobble age (8.1 $\pm$ 0.7 ka; Figs. S1E and 9) is indistinguishable from a bedrock sample (GL080; 7.9 $\pm$ 0.2 ka) and a

462 boulder sample (GL081; 7.6 $\pm$ 0.1 ka) collected from the same location (Corbett et al., 2011).
463 These observations are consistent with the findings of Briner et al. (2013), who reported cobble
464 exposure ages similar to boulder and bedrock ages in central western Greenland, a landscape
465 deeply scoured by erosive warm-based ice. However, in Upernavik, the mean surficial cobble
466 age (7.8 $\pm$ 1.6 ka; Figs. S1F and 9) is younger than a bedrock sample (GU001; 13.6 $\pm$ 0.3 ka) and
467 a boulder sample (GU002; 10.6 $\pm$ 0.3 ka) collected from the same location (Corbett et al., 2013).
468 This offset likely reflects the effect of snow or till cover on the small cobble samples and/or ^{10}Be
469 inheritance in the bedrock and boulder samples. The Upernavik area shows strong evidence for
470 non-erosive, cold-based ice (Beel et al., 2016; Corbett et al., 2013), which may lead to
471 disagreement between exposure ages inferred from bedrock, boulders, and cobbles.
472
473 **7. Conclusions**
474 Analysis of cosmogenic nuclides in 86 subglacial cobbles and 9 surficial cobbles from
475 western Greenland demonstrates that detrital material currently emerging at the ice sheet
476 margin has cosmogenic nuclide concentrations generally indicative of deep erosion. Most
477 subglacial cobbles contain little ^{10}Be, only ~10^3 atoms g^{-1}, suggesting they were sourced from
478 depth and have experienced little exposure since they were quarried. Although less erosive
479 areas of the ice sheet exist and are documented in other studies, they are not well-represented
480 in detrital sediment samples, which originate from areas of warm-based, erosive ice.
481 Measurable ^{14}C in some subglacial cobbles indicates recent nuclide production, within the past
482 ~30 ka; however, ^{14}C/^{10}Be ratios above that of surface production indicate that nuclide
483 production occurred under shielding. Only two subglacial cobbles have ^{14}C/^{10}Be and ^{14}C/^{26}Al

484 ratios indicative of excess longer-lived nuclides; their ^{10}Be and ^{26}Al concentrations can be
485 explained by surface or near-surface exposure predating the timespan recorded by ^{14}C. Surficial
486 cobbles exhibit scatter in their ^{10}Be concentrations beyond analytic uncertainties, and match
487 deglaciation age estimates better in certain areas than in others. Overall, the nuclide
488 concentrations of 95 glacial cobbles demonstrate that muon-produced nuclides are pervasive
489 even in long-buried and deeply-eroded landscapes. Although inherited ^{10}Be is generally present
490 in small concentrations, it is occasionally present in concentrations high enough to influence
491 exposures ages.

Acknowledgements
Support for this research was provided by NSF ARC-0713956, NSF ARC-1023191, a NSF Doctoral Dissertation Research Improvement Grant (BCS-1433878), and an NSF Graduate Research Fellowship. Corbett's time was partially supported by NSF EAR-1735676. Field support was provided by CH2MHILL. We thank R. Finkel for assistance with ^{10}Be measurements at Lawrence Livermore National Laboratory, performed under the auspices of the U.S. Department of Energy under contract DE-AC52-07NA27344. Work at PRIME Laboratory was supported by NSF EAR-0919759. We thank T. Dunai for conducting ^{14}C measurements at University of Cologne and two anonymous reviewers for providing feedback that improved the manuscript.

References

Alley, R., Cuffey, K., Evenson, E., Strasser, J., Lawson, D., Larson, G., 1997. How glaciers entrain and transport basal sediment: physical constraints. Quaternary Science Reviews 16, 1017-1038.

Argento, D., Reedy, R., Stone, J., 2013. Modeling the earth's cosmic radiation. Nuclear Instruments and Methods in Physics Research B 294, 464-469.

Balco, G., 2011. Contributions and unrealized potential contributions of cosmogenic-nuclide exposure dating to glacier chronology, 1990-2010. Quaternary Science Reviews 30, 3-27.

Balco, G., 2017. Production rate calculations for cosmic-ray-muon-produced ^{10}Be and ^{26}Al benchmarked against geological calibration data. Quaternary Geochronology 39, 150-173.

Balco, G., Stone, J., Sliwinsku, M., Todd, C., 2014. Features of the glacial history of the Transantarctic Mountains inferred from cosmogenic ^{26}Al, ^{10}Be and ^{21}Ne concentrations in bedrock surfaces. Antarctic Science 26, 708-723.

Balco, G., Stone, J.O., Lifton, N.A., Dunai, T.J., 2008. A complete and easily accessible means of calculating surface exposure ages or erosion rates from ^{10}Be and ^{26}Al measurements. Quaternary Geochronology 3, 174-195.

Beel, C., Lifton, N., Briner, J., Goehring, B., 2016. Quaternary evolution and ice sheet history of contrasting landscapes in Uummannaq and Sukkertoppen, western Greenland. Quaternary Science Reviews 149, 248-258.

Bierman, P., Shakun, J., Corbett, L., Zimmerman, S., Rood, D., 2016. A persistent and dynamic East Greenland Ice Sheet over the past 7.5 million years. Nature 540, 256-260.

Briner, J., Hakansson, L., Bennike, O., 2013. The deglaciation and neoglaciation of Upernavik Isstrøm, Greenland. Quaternary Research 80, 459-467.

Briner, J., Stewart, H., Young, N., Phillips, W., Losee, S., 2010. Using proglacial-threshold lakes to constrain fluctuations of the Jakobshavn Isbrae ice margin, western Greenland, during the Holocene. Quaternary Science Reviews 29, 3861-3874.

Briner, J.P., Goehring, B.M., Mangerud, J., Svendsen, J.I., 2016. The deep accumulation of ^{10}Be at Utsira, southwestern Norway: Implications for cosmogenic nuclide exposure dating in peripheral ice sheet landscapes. Geophysical Research Letters 43, 9121-9129.

Briner, J.P., Lifton, N.A., Miller, G.H., Refsnider, K., Anderson, R., Finkel, R., 2014. Using in situ cosmogenic ^{10}Be, ^{14}C, and ^{26}Al to decipher the history of polythermal ice sheets on Baffin Island, Arctic Canada. Quaternary Geochronology 19, 4-13.

Christ, A., Bierman, P., Knutz, P., Corbett, L.B., Fosdick, J., Thomas, E., Cowling, O., Hidy, A., Caffee, M., 2019. The northwestern Greenland Ice Sheet during the early Pleistocene was similar to today. Geophysical Research Letters 47, GL085176.

Colville, E., Carlson, A., Beard, B., Hatfield, R., Stoner, J., Reyes, A., Ullman, D., 2011. Sr-Nd-Pb isotope evidence for ice-sheet presence on southern Greenland During the Last Interglacial. Science 333, 620-623.

Corbett, L., Bierman, P., Rood, D., Caffee, M., Lifton, N., Woodruff, T., 2017. Cosmogenic ^{26}Al/^{10}Be Surface Production Ratio in Greenland. Geophysical Research Letters 44, 1350-1359.

Corbett, L., Young, N., Bierman, P., Briner, J., Neumann, T., Graly, J., Rood, D., 2011. Paired bedrock and boulder ^{10}Be concentrations resulting from early Holocene ice retreat near Jakobshavn Isfjord, western Greenland. Quaternary Science Reviews 30, 1739-1749.

Corbett, L.B., Bierman, P.R., Graly, J.A., Neumann, T.A., Rood, D.H., 2013. Constraining landscape history and glacial erosivity using paired cosmogenic nuclides in Upernavik, northwest Greenland. Geological Society of America Bulletin 125, 1539-1553.

Corbett, L.B., Bierman, P.R., Rood, D.H., 2016. An approach for optimizing in situ cosmogenic ^{10}Be sample preparation. Quaternary Geochronology 33, 24-34.

Cuffey, K., Paterson, W., 2010. The Physics of Glaciers, Fourth Edition ed. Academic Press.

Davis, P., Bierman, P., Marsella, K., Caffee, M., Southon, J., 1999. Cosmogenic analysis of glacial terrains in the eastern Canadian Arctic: a test for inherited nuclides and the effectiveness of glacial erosion. Annals of Glaciology 28.

De Vernal, A., Hillaire-Marcel, C., 2008. Natural variability of Greenland climate, vegetation, and ice volume during the past million years. Science 320, 1622-1625.

Flesche-Kleiven, H., Jansen, E., Fronval, T., Smith, T., 2002. Intensification of Northern Hemisphere glaciations in the circum Atlantic region (3.5–2.4 Ma) – ice-rafted detritus evidence. Palaeogeography, Palaeoclimatology, Palaeoecology 184, 213-223.

Fulop, R., Wacker, L., Dunai, T., 2015. Progress report on a novel in situ ^{14}C extraction scheme at the University of Cologne. Nuclear Instruments and Methods Section B: Beam Interactions with Materials and Atoms 361, 20-24.

Funder, S., Bennike, O., Bocher, J., Israelson, C., Petersen, K., Simonarson, L., 2001. Late Pliocene Greenland- The Kap Kobenhavn Formation in North Greenland. Bulletin of the Geological Society of Denmark 48, 117-134.

Goehring, B., Kelly, M., Schaefer, J., Finkel, R., Lowell, T., 2010. Dating of raised marine and lacustrine deposits in east Greenland using beryllium-10 depth profiles and implications for estimates of subglacial erosion. Journal of Quaternary Science 25, 865-874.

Graly, J., Corbett, L., Bierman, P., Lini, A., Neumann, T., 2018. Meteoric ^{10}Be as a tracer of subglacial processes and interglacial surface exposure in Greenland. Quaternary Science Reviews 191, 118-131.

Håkansson, L., Alexanderson, H., Hjort, C., Moller, P., Briner, J., Aldahan, A., Possnert, G., 2009. Late Pleistocene glacial history of Jameson Land, central East Greenland, derived from cosmogenic ^{10}Be and ^{26}Al exposure dating. Boreas 38, 244-260.

Heisinger, B., Lal, D., Jull, A., Kubik, P., Ivy-Ochs, S., Knie, K., Nolte, E., 2002a. Production of selected cosmogenic radionuclides by muons: 2. Capture of negative muons. Earth and Planetary Science Letters 200, 357-369.

Heisinger, B., Lal, D., Jull, A., Kubik, P., Ivy-Ochs, S., Neumaier, S., Knie, K., Lazarev, V., Nolte, E., 2002b. Production of selected cosmogenic radionuclides by muons: 1. Fast muons. Earth and Planetary Science Letters 200, 345-355.

Helland, P., Holmes, M., 1997. Surface Textural Analysis of Quartz Sand Grains from ODP Site 918 Off the Southeast Coast of Greenland Suggests Glaciation of Southern Greenland at 11 Ma. Palaeogeography, Palaeoclimatology, Palaeoecology 135, 109-121.

Helsen, M., Van De Berg, W., Van De Wal, R., Van Den Broeke, M., Oerlemans, J., 2013. Coupled regional climate–ice sheet simulation shows limited Greenland ice loss during the Eemian. Climate of the Past 9.

Lal, D., Peters, B., 1967. Cosmic Ray Produced Radioactivity on the Earth, Encyclopedia of Physics. Springer, Berlin, pp. 551-612.

Larsen, H., Saunders, A., Clift, P., Beget, J., Wei, W., Spezzaferri, S., 1994. Seven million years of glaciation in Greenland. Science 264, 952-955.

Larsen, N., Hjaer, K., Lecavalier, B., Bjork, A., Colding, S., Huybrechts, P., Jakobsen, K., Kjeldsen, K., Knudsen, K., Odgaard, B., Olsen, J., 2015. The response of the southern Greenland ice sheet to the Holocene thermal maximum. Geology 43, 291-294.

Levy, L., Kelly, M., Howley, J., Virginia, R., 2012. Age of the Ørkendalen moraines, Kangerlussuaq, Greenland: constraints on the extent of the southwestern margin of the Greenland Ice Sheet during the Holocene. Quaternary Science Reviews 52, 1-5.

Lupker, M., Hippe, K., Wacker, L., Kober, F., Maden, C., Braucher, R., Bourles, D., Vidal Romani, J., Wieler, R., 2015. Depth-dependence of the production rate of in situ ^{14}C in quartz from the Leymon High core, Spain. Quaternary Geochronology 28, 80-87.

Marrero, S., Phillips, F., Borchers, B., Lifton, N., Aumer, R., Balco, G., 2016. Cosmogenic nuclide systematics and the CRONUScalc program. Quaternary Geochronology 31, 160-187.

Miller, G.H., Briner, J.P., Lifton, N.A., Finkel, R.C., 2006. Limited ice-sheet erosion and complex exposure histories derived from in situ cosmogenic ^{10}Be, ^{26}Al, and ^{14}C on Baffin Island, Arctic Canada. Quaternary Geochronology 1, 74-85.

Nelson, A., Bierman, P., Shakun, J., Rood, D., 2014. Using in situ cosmogenic ^{10}Be to identify the source of sediment leaving Greenland. Earth Surface Processes and Landforms 39, 1087-1100.

Petrunin, A., Rogozhina, I., Vaughan, A., Kukkonen, I., Kaban, M., Koulakov, I., Thomas, M., 2013. Heat flux variations beneath central Greenland/'s ice due to anomalously thin lithosphere. Nature Geoscience 6, 746-750.

Rand, C., Goehring, B., 2019. The distribution and magnitude of subglacial erosion on millennial timescales at Engabreen, Norway. Annals of Glaciology 60, 73-81.

Reyes, A., Carlson, A., Beard, B., Hatfield, R., Stoner, J., Winsor, K., Welke, B., Ullman, D., 2014. South Greenland ice-sheet collapse during Marine Isotope Stage 11. Nature 510, 525-528.

Schaefer, J., Finkel, R., Balco, G., Alley, R., Caffee, M., Briner, J., Young, N., Gow, A., Schwartz, R., 2016. Greenland was nearly ice-free for extended periods during the Pleistocene. Nature 540, 252-255.

Schimmelpfennig, I., Schaefer, J., Goehring, B., Lifton, N., Putnam, A., Barrell, D., 2012. Calibration of the in situ cosmogenic ^{14}C production rate in New Zealand's Southern Alps. Journal of Quaternary Science 27, 671-674.

Strunk, A., Knudsen, M., Egholm, D., Jansen, J., Levy, L., Jacobsen, B., Larsen, N., 2017. One million years of glaciation and denudation history in west Greenland. Nature Communications 8.

Young, N., Briner, J., Rood, D., Finkel, R., Corbett, L., Bierman, P., 2013. Age of the Fjord Stade moraines in the Disko Bugt region, western Greenland, and the 9.3 and 8.2 ka cooling events. Quaternary Science Reviews 60, 76-90.

Table and Figure Captions

Table 1. Isotopic concentrations and uncertainties for the cobbles with ^{10}Be, ^{26}Al, and ^{14}C data. All 95 ^{10}Be measurements are shown in Table S1. Analysis details including measured ratios, background-corrected ratios, AMS cathode numbers, and primary standards are shown in Tables S1 (for ^{10}Be), S2 (for ^{26}Al), and S4 (for ^{14}C). Blanks for ^{10}Be and ^{26}Al are detailed in Table S3.

Figure 1. Map of Greenland showing the three locations from which cobble-sized rocks were collected from the present-day ice sheet margin. "Icebound" cobbles were embedded directly in the ice, whereas "outwash" cobbles are from large outwash tunnels proximal to the ice sheet margin; both are "subglacial". Conversely, "surficial" cobbles are from the proglacial landscape and have presumably been exposed since deglaciation. Also shown are other cosmogenic isotope records of detrital sediments as discussed in the text.

Figure 2. Theoretical models of ^{10}Be production (dark gray lines) and ^{14}C production (light gray lines) by both spallation (thick lines) and muons (thin lines) as a function of depth. Shown also is the resulting ^{14}C/^{10}Be ratio (heavy black line). Depth is expressed in terms of mass depth. All curves assume sea level production in central western Greenland. ^{14}C spallation production rates are derived from measurements of CRONUS-A material extracted in the Tulane cosmogenic nuclide lab (B.M. Goehring, unpublished data, n = 20), and ^{14}C muon production rates are from (Balco, 2017).

Figure 3. Probability density function of ^{10}Be concentrations of subglacial cobbles (n = 73 above detection limit). Thin gray lines represent the measured isotopic concentrations and internal uncertainties for each sample; thick black line represents the summed probability. Sample names are shown for the cobbles with the highest ^{10}Be concentrations (see Table 1 for detail). Inset: Histogram of ^{10}Be concentrations of the 86 subglacial cobbles we analyzed for ^{10}Be (including 13 that were below detection limit); note logarithmic scale on the x-axis.

Figure 4. Box plots based on four different metrics (location, type, angularity, and lithology) for describing the ^{10}Be concentrations of the subglacial cobbles. Each population includes 73 total subglacial cobbles that were above detection limit for ^{10}Be. The heavy black line shows the mean, while the dashed black line shows the median; the top and bottom of the box show the mean $\pm$ 1SD.

Figure 5. ^{26}Al-^{10}Be paired nuclide plot for 13 subglacial cobbles. The thick and thin black curves show the continuous exposure pathway and steady-states with respect to steady erosion endpoints respectively for the Greenland ^{26}Al/^{10}Be production ratio of 7.3 (based on Corbett et al. (2017)). The thick and thin gray curves show the constant production pathway and erosion

endpoints for the commonly-assumed $^{26}Al/^{10}Be$ production ratio of 6.75. Error bars show +/- 1SD.

Figure 6. Paired $^{14}C/^{10}Be$ plot for 10 subglacial cobbles with detectable ^{14}C presented in terms of production rate normalized $^{14}C/^{10}Be$ ratio and ^{10}Be concentrations. Normalization was made assuming the ^{14}C and ^{10}Be production rates for sea level and high latitude. Error ellipses are shown at the 68% confidence level. All but two of the samples plot above the field of continuous exposure, one sample is consistent with continuous exposure, and another sample is consistent with at least one period of exposure and burial.

Figure 7. Linear regressions of ^{14}C concentration versus ^{10}Be concentration (top panel, n = 10) and ^{26}Al concentration (bottom panel, n = 9) for subglacial cobbles. Regressions are for samples symbolized with gray dots; those with white dots (samples with ^{10}Be below detection limit) and black dots (samples enriched in the long-lived isotopes) are not included in the regression.

Figure 8. Simulated ^{10}Be concentrations and $^{26}Al/^{10}Be$ ratios for Pleistocene exposure scenarios #1 (dark gray) and #2 (light gray) from Schaefer et al. (2016). The two bars at the top show exposure scenarios, with burial during gray intervals and exposure during white intervals. The upper panel shows the simulated ^{10}Be concentrations and $^{26}Al/^{10}Be$ ratios at the surface of a bedrock column subjected to glacial erosion rates ranging from 5 to 50 m Myr^{-1} under thick ice cover (i.e., no production during burial intervals). Nuclide concentrations in the bedrock column were in steady state with 20 m Myr^{-1} erosion at the start of the simulations; different pre-glacial erosion rates would shift the curves up or down only modestly by the end of each simulation. The kernel density estimates along the left side of the figure show our measured glacial cobble data (as in Fig. 3). The lower panel is the same as the upper panel, but simulates low-level nuclide production by muons through thin, 50-m ice cover during burial intervals. For individual views of any of the above simulations, see Figs. S1 and S2.

Figure 9. ^{10}Be concentrations (top panel) and inferred exposure ages (bottom panel) of surficial cobbles from well outside the modern-day ice margin (n = 3 per site, detail in Table S5). Cobbles at each site were collected from the same location, all within several meters of one another. Error bars show 1σ analytic uncertainties (not visible in all cases). Gray lines show the average concentration/age at each site, and the gray box shows $\pm$ 1SD. Dashed lines denote comparisons. Photographs of the sites at which cobbles, the bedrock surface, and a boulder were all sampled are shown in Fig. 2E (Ilulissat) and 2F (Upernavik).

Sample Name	^{10}Be Concentration (atoms g^{-1})[a]	1σ ^{10}Be Uncertainty (atoms g^{-1})[a]	^{26}Al Concentration (atoms g^{-1})[b]	1σ ^{26}Al Uncertainty (atoms g^{-1})[b]	^{26}Al/^{10}Be Ratio	1σ ^{26}Al/^{10}Be Uncertainty	^{14}C Concentration (atoms g^{-1})[c]	1σ ^{14}C Uncertainty (atoms g^{-1})[c]	^{14}C/^{10}Be Ratio	1σ ^{14}C/^{10}Be Uncertainty
GK015	3.26E+04	5.67E+02	2.16E+05	1.30E+04	6.64	0.42	8.32E+04	8.60E+03	2.56	0.27
GK022	1.10E+04	3.09E+02	7.28E+04	4.44E+03	6.64	0.45	1.24E+05	9.50E+03	11.31	0.92
GK040	4.85E+03	4.25E+02	2.41E+04	4.95E+03	4.98	1.11	6.48E+04	1.74E+04	13.37	3.78
GK051	8.32E+03	2.76E+02	ND	ND	ND	ND	9.09E+04	2.52E+04	10.92	3.05
GK070	4.29E+03	3.04E+02	3.44E+04	3.06E+03	8.03	0.91	BDL	BDL	ND	ND
GK071	4.06E+03	2.25E+02	3.08E+04	4.31E+03	7.59	1.14	7.90E+04	8.70E+03	19.45	2.40
GK072	3.53E+03	1.68E+02	2.34E+04	2.96E+03	6.61	0.89	BDL	BDL	ND	ND
GK097	1.82E+04	4.12E+02	1.37E+05	1.18E+04	7.52	0.67	ND	ND	ND	ND
GK099	1.18E+04	3.09E+02	8.67E+04	6.85E+03	7.37	0.61	BDL	BDL	ND	ND
GL028	5.00E+03	2.08E+02	2.97E+04	2.61E+03	5.93	0.58	6.91E+04	9.10E+03	13.81	1.91
GL036	3.99E+03	2.15E+02	3.34E+04	4.40E+03	8.38	1.19	6.60E+04	8.50E+03	16.55	2.31
GU010	1.12E+05	2.23E+03	7.71E+05	2.51E+04	6.87	0.26	5.10E+04	1.37E+04	0.45	0.12
GU034	7.38E+03	3.94E+02	3.92E+04	3.21E+03	5.31	0.52	7.81E+04	9.00E+03	10.58	1.34
GU126	1.89E+04	4.18E+02	1.42E+05	1.18E+04	7.52	0.65	1.51E+05	1.50E+04	8.00	0.81

[a]The ^{10}Be/^{9}Be measurements were made at Lawrence Livermore National Laboratory and were normalized to standard 07KNSTD3110 with an assumed ratio of 2.85 x 10^{-11} (Nishiizumi et al., 2007).

[b]The ^{26}Al/^{27}Al measurements were made at Purdue Rare Isotope Measurement Laboratory and were normalized to standard KNSTD with an assumed ratio of 1.818 x 10^{-12} (Nishiizumi et al., 2004).

[d]The ^{14}C measurements were made at University of Cologne.

ND = No data (sample failed during measurement yielding no usable data)

BDL = Below detection limit (see text for details)

Table 1.

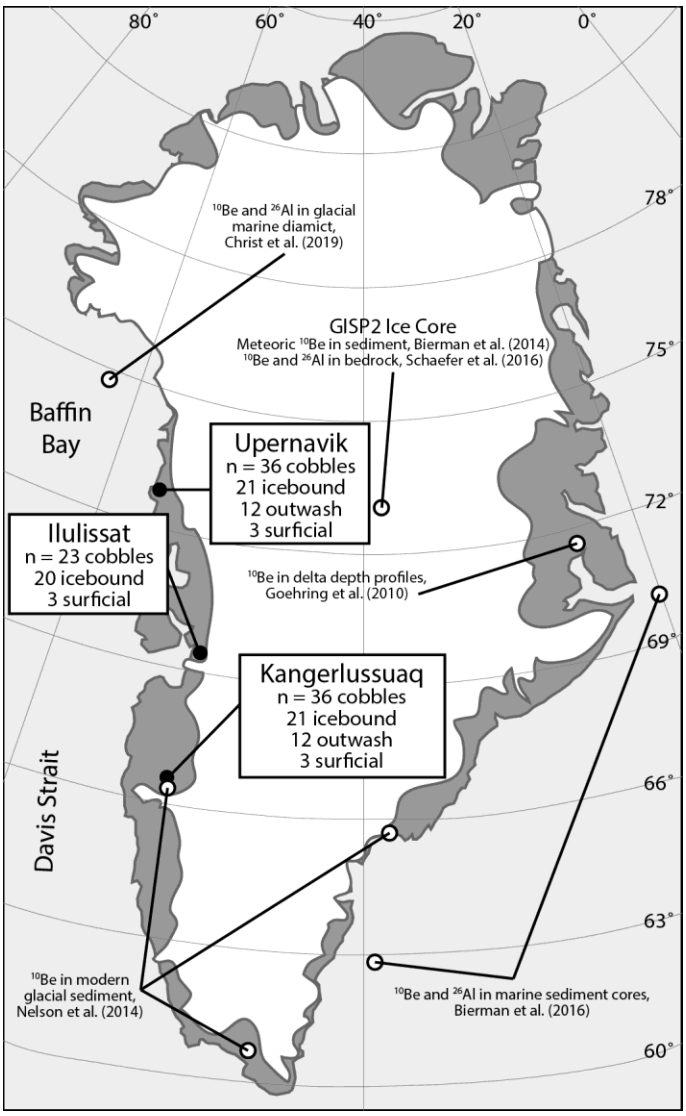

Figure 1.
(Width = 90mm, one column)

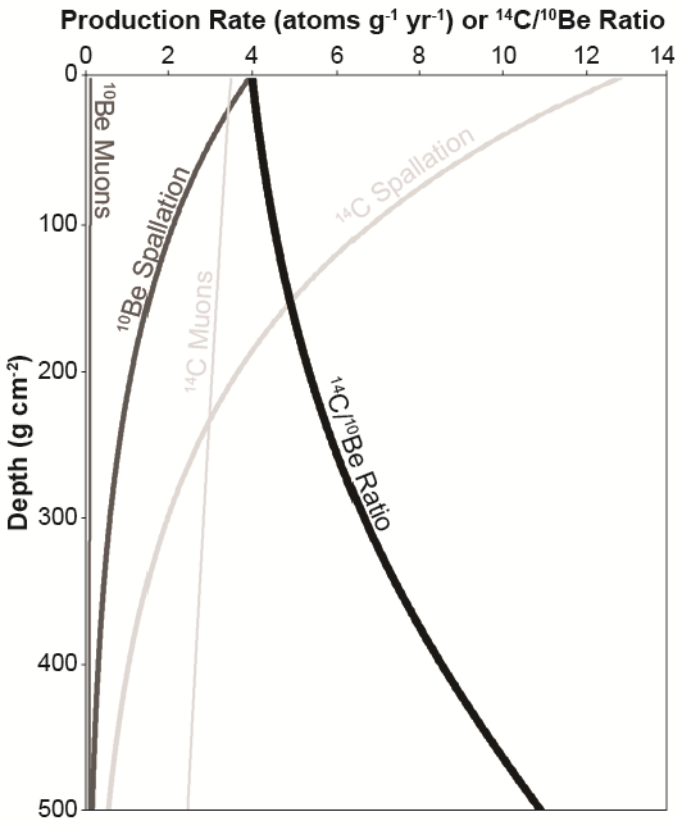

Figure 2.
(Width = 90 mm, one column)

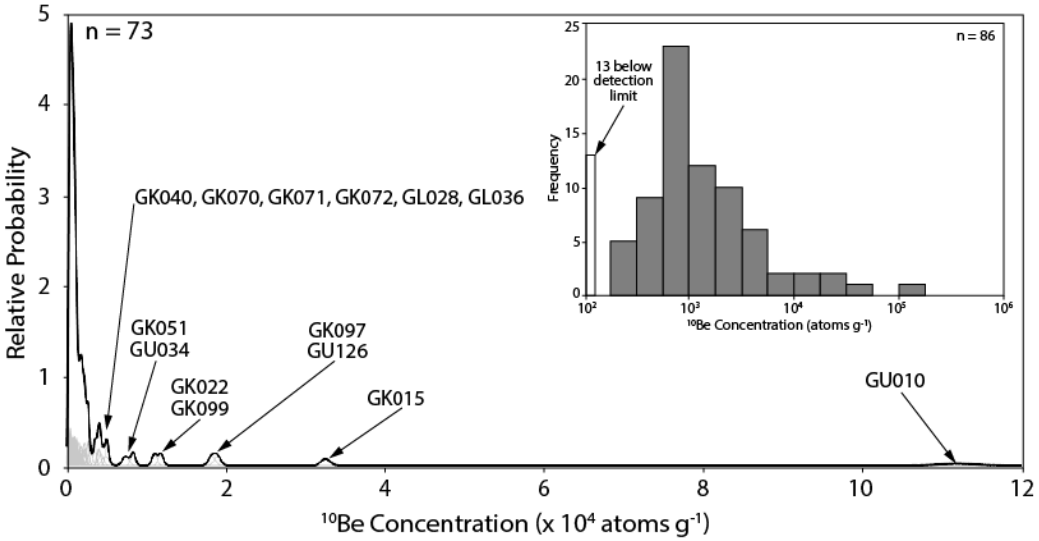

Figure 3.
(Width = 140 mm, 1.5 columns)

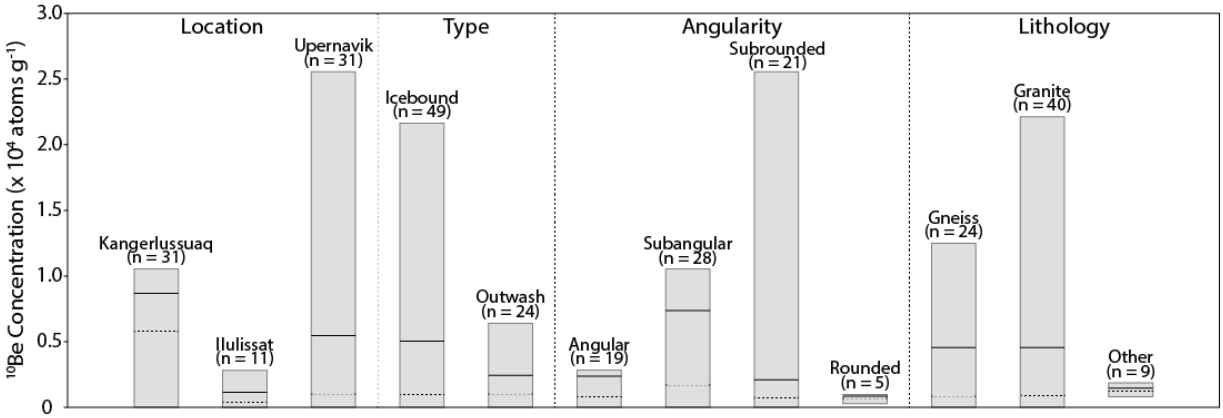

Figure 4.
(Width = 190 mm, full page)

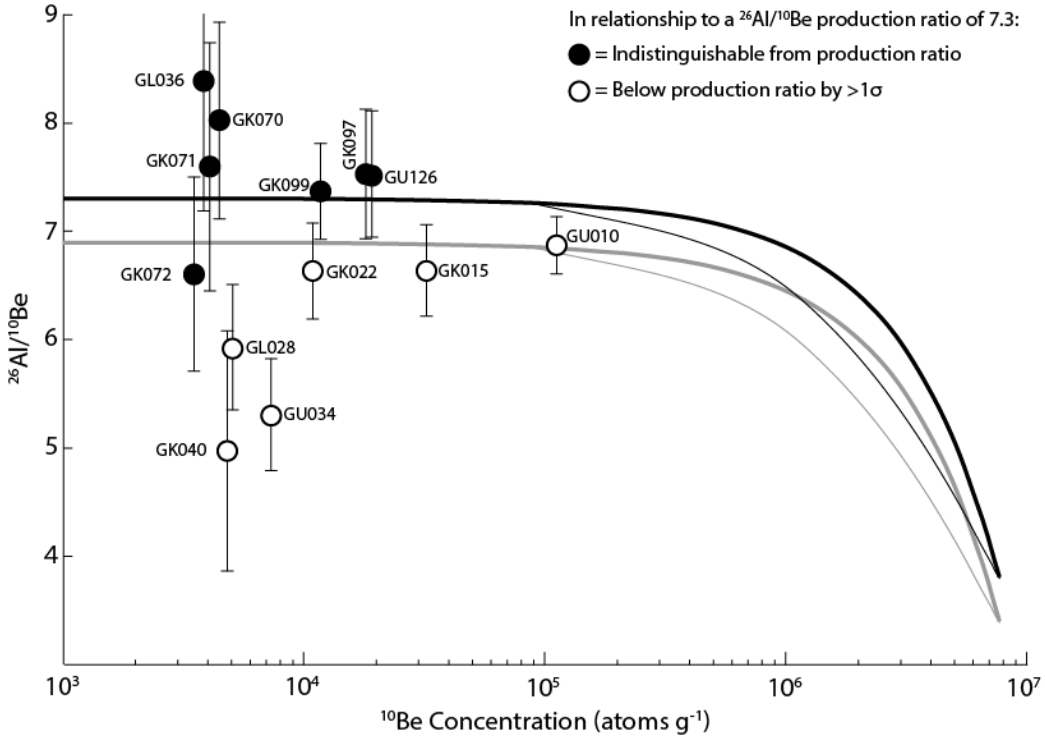

Figure 5.
(Width = 140 mm, 1.5 columns)

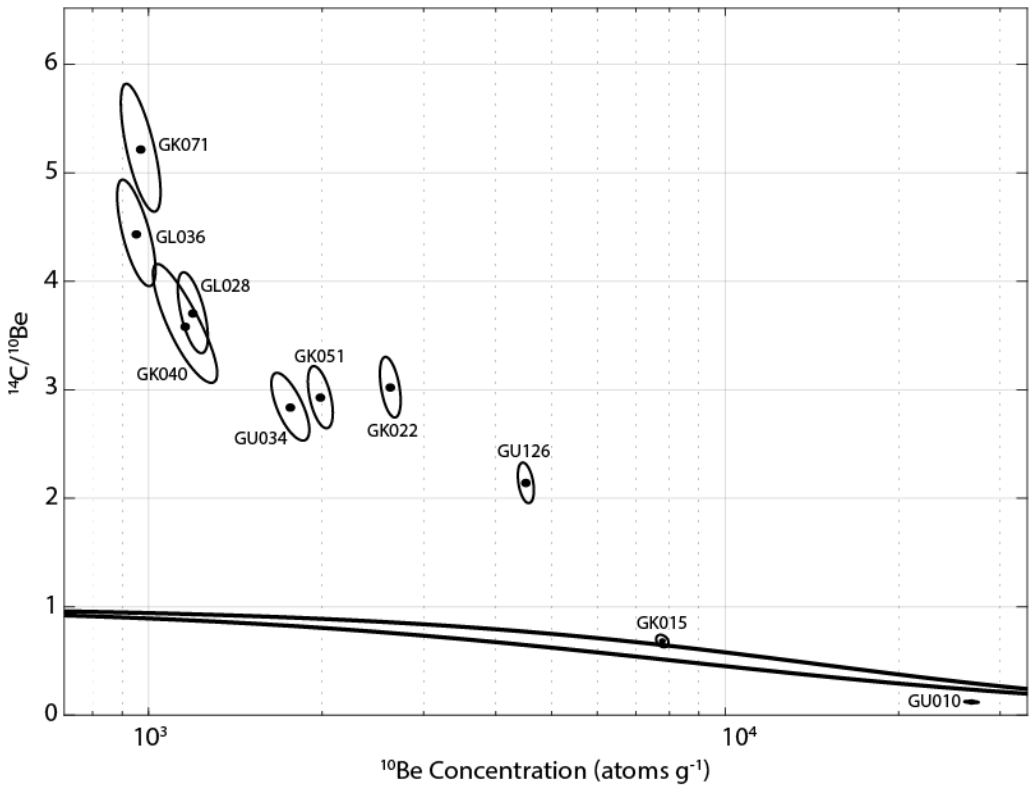

Figure 6.
(Width = 140 mm, 1.5 columns)

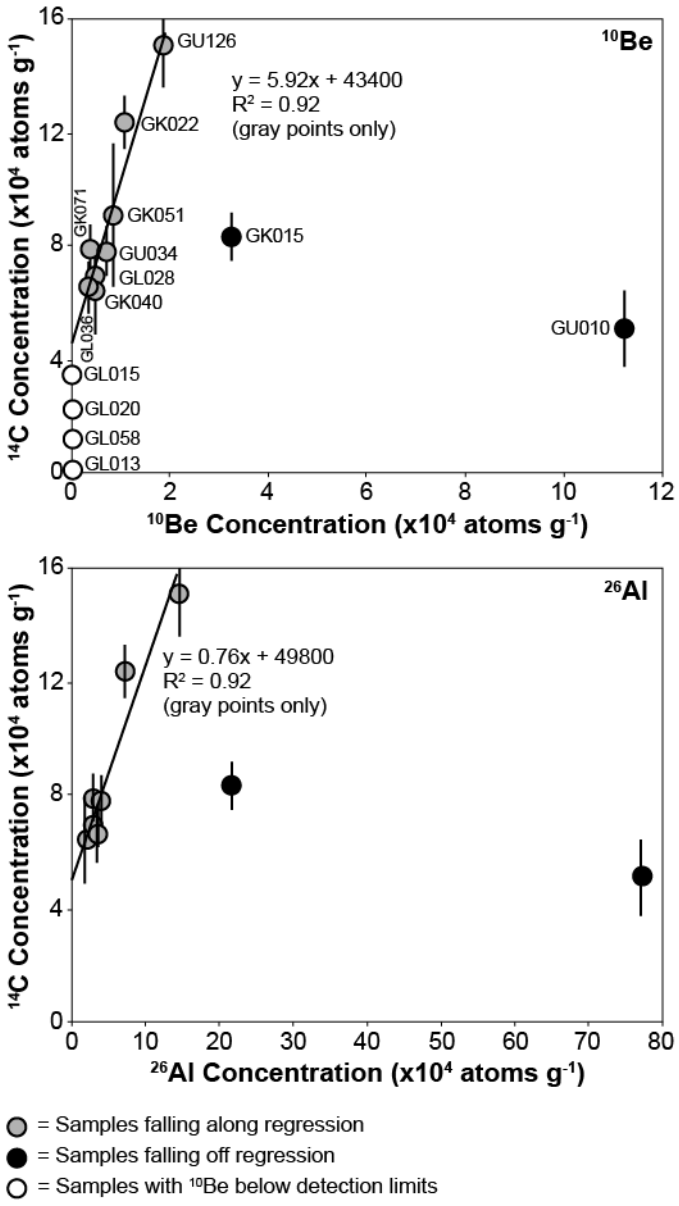

Figure 7.
(Width = 90mm, one column)

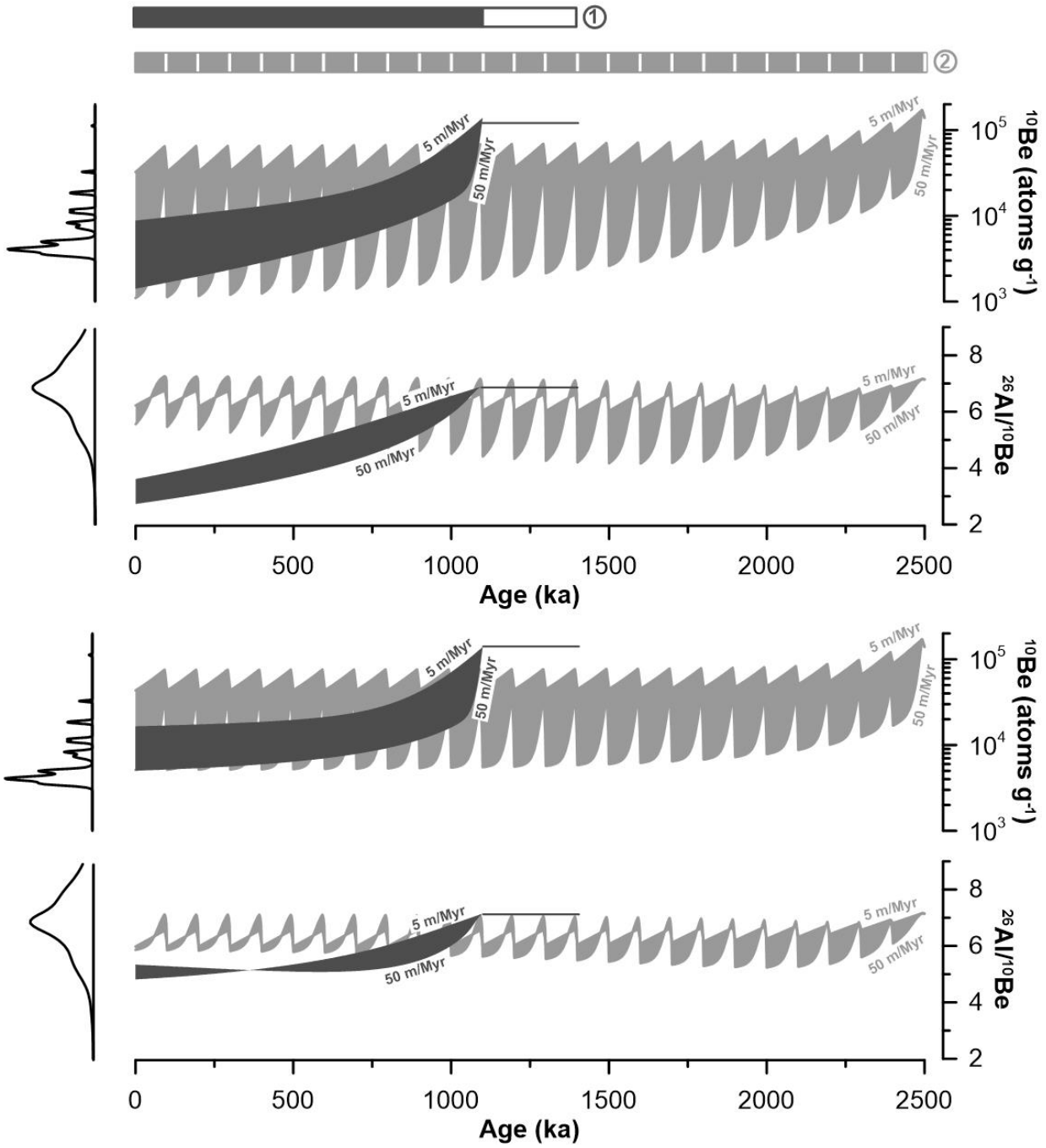

Figure 8.
(Width = 140 mm, 1.5 columns)

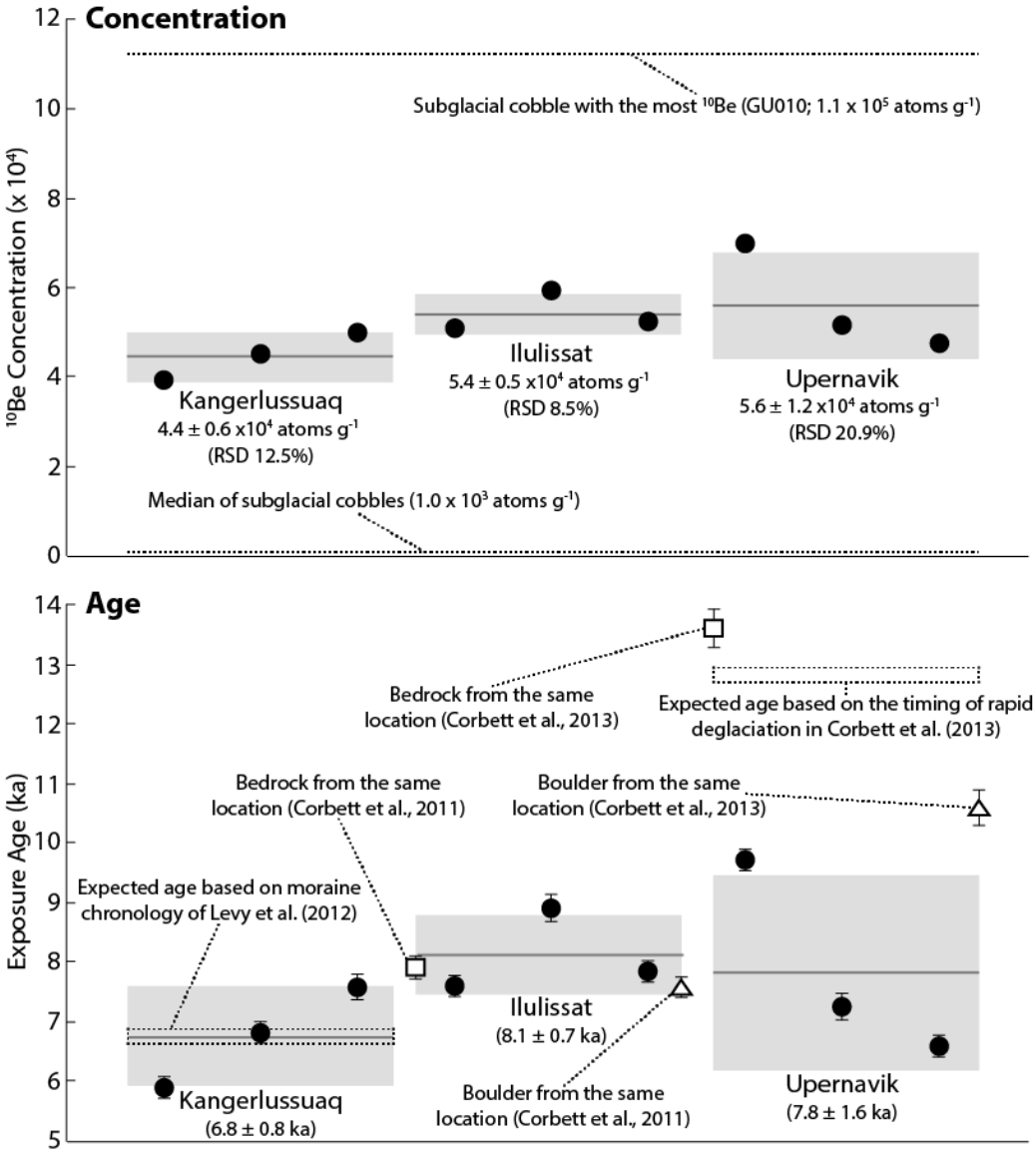

Figure 9.
(Width = 140 mm, 1.5 columns)